

## Discovery of Pyridyl Bis(oxy)dibenzimidamide Derivatives as Selective Matriptase Inhibitors

Rajeev Goswami,<sup>†</sup> Subhendu Mukherjee,<sup>†</sup> Gerd Wohlfahrt,<sup>‡</sup> Chakshumathi Ghadiyaram,<sup>†</sup> Jwala Nagaraj,<sup>†</sup> Beeram Ravi Chandra,<sup>†</sup> Ramesh K. Sistla,<sup>†</sup> Leena K. Satyam,<sup>†</sup> Dodheri S. Samiulla,<sup>†</sup> Anu Moilanen,<sup>§</sup> Hosahalli S. Subramanya,<sup>†</sup> and Murali Ramachandra<sup>\*,†</sup>

<sup>†</sup>Aurigene Discovery Technologies Limited, 39-40 KIADB Industrial Area, Electronic City Phase II, Bangalore 560 100, India

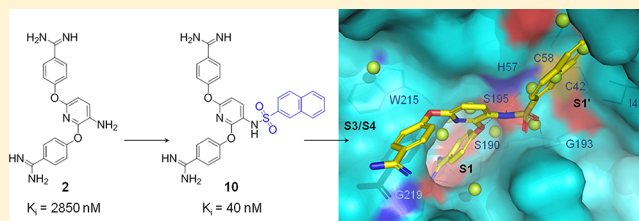
<sup>‡</sup>Orion Corporation, Orionintie 1, FIN-02101 Espoo, Finland

<sup>§</sup>Orion Corporation, Tengströminkatu 8, FIN-20101 Turku, Finland

### Supporting Information

**ABSTRACT:** Matriptase belongs to trypsin-like serine proteases involved in matrix remodeling/degradation, growth regulation, survival, motility, and cell morphogenesis. Herein, we report a structure-based approach, which led to the discovery of sulfonamide and amide derivatives of pyridyl bis(oxy)-benzimidamide as potent and selective matriptase inhibitors. Co-crystal structures of selected compounds in complex with matriptase supported compound designing. Additionally, WaterMap analyses indicated the possibility of occupying a distinct pocket within the catalytic domain, exploration of which resulted in >100-fold improvement in potency. Co-crystal structure of **10** with matriptase revealed critical interactions leading to potent target inhibition and selectivity against other serine proteases.

**KEYWORDS:** Matriptase, pyridyl dibenzimidamide, SAR, crystal structure, cancer



Metastasis is the principal event leading to death in individuals with cancer.<sup>1</sup> Progression of metastasis embraces complex processes that require multiple proteolytic steps for degradation and remodeling of the extracellular matrix. Because proteases from diverse classes are involved in these mechanisms,<sup>2–5</sup> a possible approach to prevent tumor growth and progression is by the use of specific protease inhibitors.<sup>6–8</sup>

Matriptase or MT-SP1 is a type II transmembrane serine protease (TTSP) that is mainly expressed in the epidermis, thymic stroma, and other epithelia.<sup>9,10</sup> The proteolytic activity of matriptase is controlled by hepatocyte growth factor activator inhibitor-1 (HAI-1).<sup>9,10</sup> Knockout mouse studies have revealed that matriptase plays a role in terminal differentiation of epidermis, hair follicle development, and thymic homeostasis.<sup>9</sup> Relative ratio of matriptase to HAI-1 is reported to be higher in a range of epithelial tumors, in which active matriptase plays an important role in cellular invasion and metastasis.<sup>11,12</sup> Matriptase is known to be overexpressed in inflammatory conditions such as osteoarthritis,<sup>13</sup> but downregulated in inflamed colonic tissues from Crohn's disease and ulcerative colitis patients.<sup>14</sup> Recent findings suggest that matriptase activates hemagglutinin of H9N2 and H1N1 influenza A viruses and promotes viral replication.<sup>15,16</sup> Matriptase is also known to activate proteases such as receptor-bound urokinase-type plasminogen activator (uPA), which plays a critical role in angiogenesis, tumor invasion, and metastasis. Down-regulation of matriptase inhibits tumor invasion through suppression of uPAR activation.<sup>17,18</sup>

Altogether, these findings imply that matriptase is a good target for the development of anticancer drugs.

Compounds for matriptase inhibition including bis-benzamidines,<sup>19</sup> amidinophenylalanines,<sup>8,20</sup> and peptidomimetics<sup>21</sup> have been reported earlier. Here we describe the discovery of bis-benzimidamide based inhibitors that were conceptualized by structure-guided design strategies. Initial design ideas were drawn from a high-resolution crystal structure of matriptase catalytic domain in complex with benzimidamide<sup>22</sup> (Figure 1).

From the binding mode of benzimidamide as sulfate salt (PDB code: 1EAX),<sup>22</sup> it was apparent that benzimidamide binds to S1 pocket forming a salt-bridge interaction with the side-chain carboxylate of Asp189 in addition to a number of hydrogen bonding contacts directly or indirectly with different residues in the vicinity such as Ser190, Gly219, and Lys224. Interestingly, this structure also revealed the position of a sulfate ion close to the benzimidamide binding site, which has hydrogen bonding interactions with catalytic residues His57, Ser195, and Gly193 either directly or mediated via water molecules. This crystal structure revealed opportunity for incorporating substituents to a benzimidamide core to extend toward the spacious and solvent exposed S3/S4 pocket close to Trp215.

Additionally, screening of a benzimidamide focused compound library of known protease inhibitors resulted in identification of **1**

Received: June 17, 2013

Accepted: October 7, 2013

Published: October 7, 2013

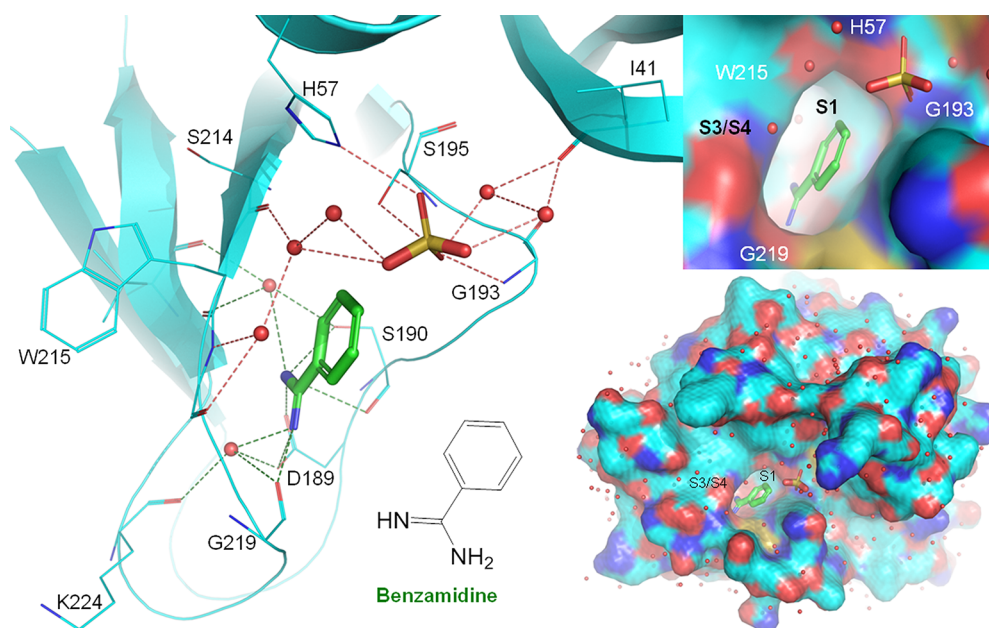


**Figure 1.** Crystallographic binding mode of benzamidine and a sulfate ion in matriptase catalytic domain (PDB code: 1EAX). Benzamidine showed a  $K_i \approx 400 \mu\text{M}$  for matriptase inhibition.

(Table 1) with a  $K_i$  value of  $9.6 \mu\text{M}$  for matriptase. Compound **1** is one of the archetypical inhibitors of serine proteases previously described as an inhibitor of factor Xa ( $K_i = 0.4 \mu\text{M}$ ), thrombin ( $K_i = 0.6 \mu\text{M}$ ), and trypsin ( $K_i = 2.8 \mu\text{M}$ ).<sup>23</sup> Further screening of pyridyl-substituted derivatives led to the identification of aminopyridine **2** with a  $K_i$  value of  $2.9 \mu\text{M}$  for matriptase but low selectivity against other proteases.

Structural modeling of **2** in the benzamidine binding pocket (Figure 2a) suggested additional hydrogen bonding possibilities with Ser195 and Gly216 apart from S1 pocket contacts similar to benzamidine. These observations for **2** motivated us to explore additional engagement of the sulfate ion binding pocket to enhance the affinity. Thus, a 3-amino group focused library with various aryl and heteroaryl sulfonamides was synthesized, and chemistry of **2** and **8** is outlined in Scheme 1. Treatment of 2,6-dichloro-3-nitropyridine with 4-hydroxybenzointrile yielded **3**, followed by reduction of nitro to amine (**4**), which was sulfonated using 4-fluorobenzenesulfonylchloride with DIPEA (*N,N*-diisopropylethylamine) in THF and this, resulted in sulfonamide derivative **5**. Refluxing nitrile intermediate **5** with  $\text{NH}_2\text{OH}\cdot\text{HCl}$  in EtOH converted to *N*-hydroxyamidine (**6**), followed by acetylation to form *N*-acetoxyamidine (**7**), which was reduced to amidine analogue **8** using zinc. Zinc was used to avoid dehalogenated side product resulting under the hydrogenation conditions. Compounds **9–11** were prepared utilizing the same synthetic route as **8** using different aryl sulfonamides. In contrast, intermediate **3** was separately subjected for conversion of its nitrile to amidine and nitro to amine in situ during hydrogenation of *N*-acetoxyamidine to afford **2**.

Newly synthesized compounds were evaluated for potency and selectivity (see Supporting Information) (Table 1).

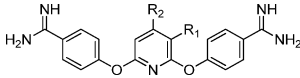
Compound **8** with 4-fluorophenyl extending toward the sulfate ion binding site showed improvement in matriptase inhibition ( $K_i$  of  $0.2 \mu\text{M}$ ). A high resolution crystal structure of **8** (PDB code: 4JZ1) in complex with matriptase showed that the compound binds in the known substrate binding pocket similar to other known prototype matriptase inhibitors<sup>8,22</sup> indicating that **8** is a competitive inhibitor. The crystal structure

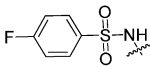
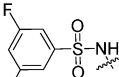
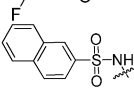
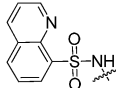
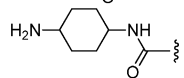
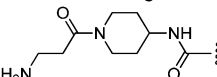
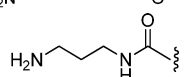
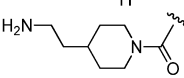
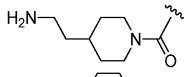
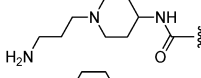
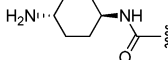
also revealed conformational similarity of the pyridinyl bis-oxy-dibenzimidamide moieties (docked model of **2** and binding mode of **8**) except for the P3/P4 benzamidine, which rotate slightly inward resulting in a backbone contact with Phe97 in the 90-loop region (Figure 2b). The sulfone moiety of **8** occupies the sulfate ion binding site making similar interactions, and the fluoro-phenyl moiety was found to be packing against the Cys42-Cys58 disulfide-bridge and Ile41 side-chain.

The crystallographic binding mode of **8** revealed opportunities for binding affinity improvement through better van der Waals (vdW) contacts with Cys42-Cys58 disulfide-bridge and Ile41. Toward predicting the impact of such interactions on binding affinity, we applied a new computational method, WaterMap by Schrödinger LLC,<sup>26</sup> which maps the arrangement and thermodynamic properties of water molecules that might solvate binding sites. This method also estimates the entropic and enthalpic forces involved in binding of small molecules and hence help to elucidate the ability of inhibitors to differentially displace specific water molecules from binding sites. WaterMap based predictions have supported the rational design of enzyme inhibitors in recent publications.<sup>27</sup>

Initially, we investigated whether the WaterMap model generated for **8** crystal structure (Figure 2c) could explain binding affinity differences between benzamidine, **2**, and **8**. From Figure 2c, we can see that 4–5 unstable water sites ( $\Delta G > 2 \text{ kcal/mol}$ ) are mapped collectively in the vicinity of 3 regions, (i) ether linker to the P1 benzamidine, (ii) pyridyl moiety, and (iii) P3/P4 benzamidine, suggesting that appending the pyridinyl bis-oxy-benzamidine to P1 benzamidine is likely to displace unstable water molecules resulting in free energy gain. Consistent with this notion,  $K_i$  improved by >100-fold when changed from benzamidine to **2**. Figure 2c also shows unstable water sites in the area occupied by the fluorophenyl sulfone substituent of **8** while filling the hydrophobic S1' region, thereby explaining the 13-fold binding difference between compounds **2** and **8**. Furthermore, we could see an unstable water site close to the fluorine atom in **8** ( $\approx 2.4 \text{ \AA}$ ) with more accessible space in the S1' region suggesting that the fluorine could be replaced by a bulkier group (Figure 2c).

Table 1. SAR of Pyridyl Bis(oxy)benzamidines



ID	R <sub>1</sub>	R <sub>2</sub>	K <sub>i</sub> <sup>a</sup> (μM)				
			Matriptase	uPA	Factor Xa	Thrombin	Trypsin
1	H	H	9.6	NA	0.4 <sup>b</sup>	0.6 <sup>b</sup>	2.8 <sup>b</sup>
2	NH <sub>2</sub>	H	2.9	>10	1.2	4.4	5.5
8		H	0.2	>10	0.3	4.1	1.4
9		H	1.2	>10	NA	NA	NA
10		H	0.04 <sup>d</sup>	>10	0.3	5.8	1.3
11		H	0.2	>10	NA	NA	NA
18		H	0.5	>10	0.6	3.4	2.0
19		H	0.6	>10	2.3	3.6	NA
20		H	0.4	>10	0.3	2.1	0.3
21		H	0.2	>10	1.5	>2.5 <sup>c</sup>	3.6
22	H		0.1	>10	0.2	>2.5 <sup>c</sup>	2.2
23	H		0.04 <sup>d</sup>	>10	0.1	2.9	NA
24	H		0.04 <sup>d</sup>	>10	0.4	2.5	2.4

<sup>a</sup>Average of two values obtained from two independent dose response studies with standard deviation within  $\pm 10\%$ . <sup>b</sup>Values from ref 23; NA indicates that the compound was not screened against the mentioned enzyme. <sup>c</sup>Indicates that  $K_i$  was not determined because of poor dose response in biochemical assay. <sup>d</sup>Reported with two decimal places and one significant digit because of the high binding affinity ( $K_i < 0.05 \mu\text{M}$ ) of these compounds

Hence, a compound was synthesized replacing the fluoro-phenyl in **8** with a naphthyl to obtain **10**, which exhibited a  $K_i$  of  $0.04 \mu\text{M}$ . Interestingly, **11** with a slightly different arrangement of the bicyclic aryl moiety (R, Table 1) that would not have mapped onto the unstable water in vicinity of **8** fluorine did not show any improvement in binding. A high resolution crystal structure of the most potent compound in this series, **10** (PDB code: 4JYT) in matriptase catalytic domain was solved, which revealed a similar binding mode as **2** (Figure 2d), thereby validating the working hypothesis of hit generation. Additionally, orientation of the P3/P4 benzamidine in the crystal structure of **10** was similar to the docked model of **2** (Figure 2a) indicating that the Phe97 interaction observed in the binding mode of **8** may not be so critical for binding. The naphthyl was also observed to make vdW contacts with Cys42-Cys58 disulfide-bridge and Ile41 as predicted. These findings indicate that, apart from S1 region polar interactions, adequate S1' region occupancy and vdW contacts could be vital for greater potency.

The crystallographic binding mode of **10** was further utilized for understanding the structural basis for selectivity against other serine proteases, factor Xa, and thrombin. This structure shows that the naphthyl moiety orients toward the 60-loop region (Figure 2e) adjacent to Cys42-Cys58 disulfide-bridge. These loop regions have different lengths and adopt diverse conformations in different serine proteases. From structural comparison of matriptase with factor Xa and thrombin, we concluded that the observed selectivity could be due to the clash of the naphthyl group with Gln61 in factor Xa and Trp60D and Lys60F in thrombin (Figure 2e) due to conformational differences of the 60-loop regions. From the crystal structure of **10**, it appeared that the aryl sulfonamide group may be replaceable with carboxamide and that extended saturated substituents could be coupled in order to reach the 60-loop region while occupying the region close to Cys42-Cys58 disulfide-bridge. Thus, a focused library of compounds with various alkyl amines

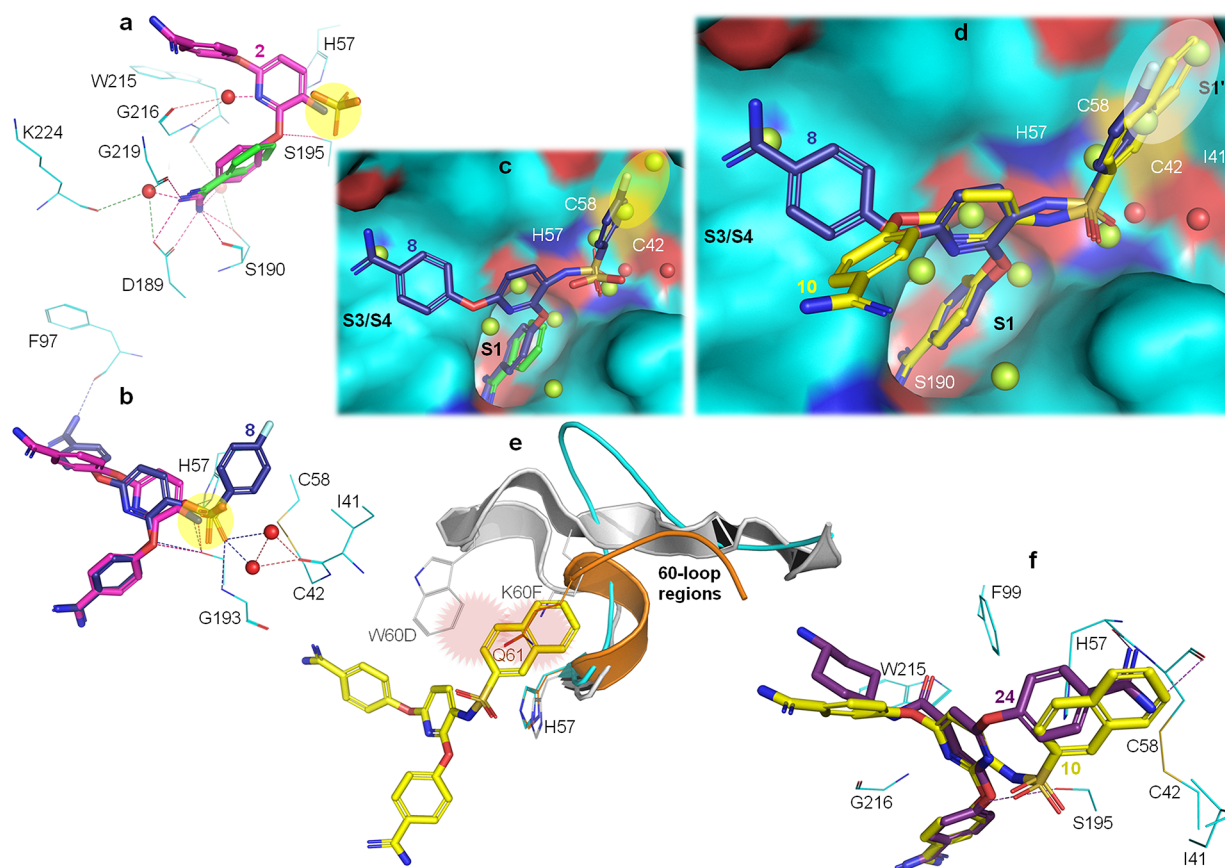


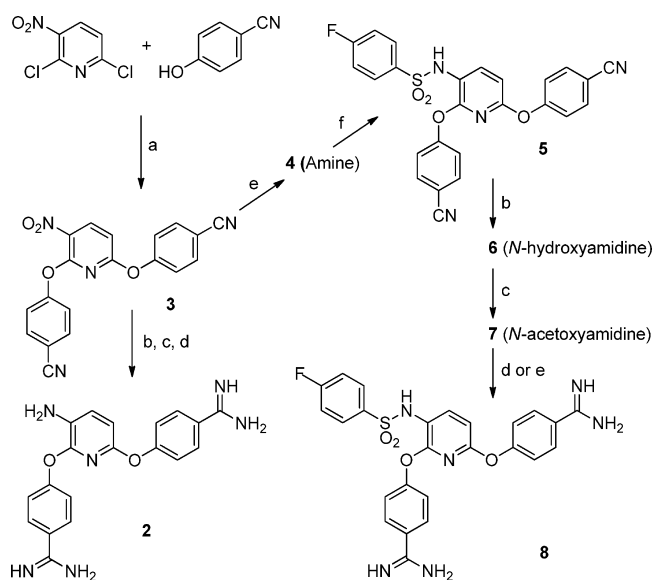
**Figure 2.** Overlays: (a) docked model of **2** ( $K_i = 2.9 \mu\text{M}$ ) and benzamidine ( $K_i \approx 400 \mu\text{M}$ ) binding mode; (b) docked model of **2** against crystallographic binding mode of **8** ( $K_i = 0.2 \mu\text{M}$ ); (c) binding modes of **8** against that of benzamidine in surface mode depicting unstable WaterMap sites. Color codings for spherical (water) representations: red, crystallographic water molecules and lemon green, unstable water sites ( $\Delta G > 2 \text{ kcal/mol}$ ); (d) Overlay of **8** and **10** crystallographic binding modes in matriptase catalytic domain along with mapped water molecules; (e) crystallographic binding mode of **10** in matriptase catalytic domain and structural basis for selectivity against thrombin (gray; PDB code: 1EB1<sup>24</sup>) and factor Xa (orange; PDB code: 1EZQ<sup>25</sup>); (f) crystallographic binding modes of **10** and **24** in matriptase catalytic domain.

was synthesized following the synthetic route described in Scheme 2.

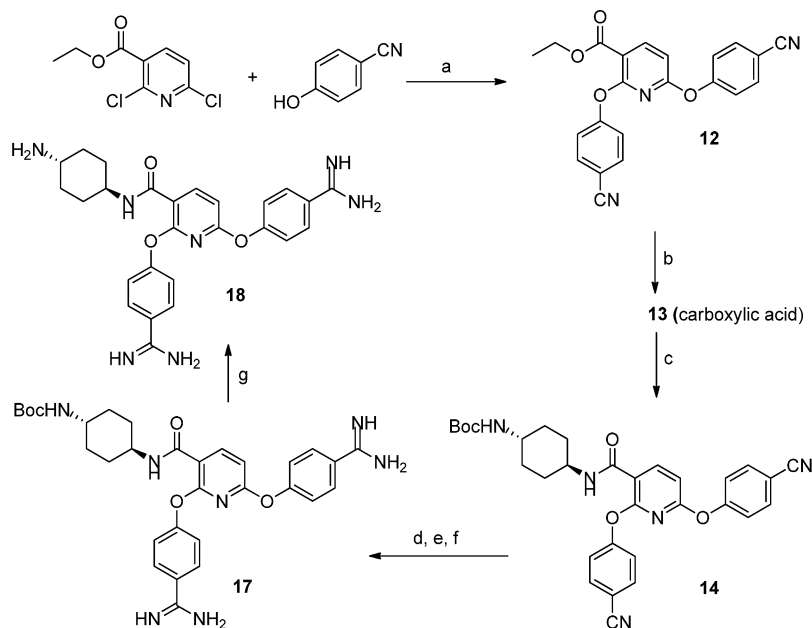
Treatment of ethyl 2,6-dichloronicotinate with 4-hydroxybenzonitrile resulted in ester **12**, which was hydrolyzed using LiOH to obtain acid **13**. *tert*-Butyl ((1*R*,4*R*)-4-aminocyclohexyl)-carbamate was coupled with **13** using benzotriazol-1-yl-oxypyrrolidinophosphonium-hexafluorophosphate (PyBop) to obtain **14**. Following the method described in Scheme 1 except using aq.  $\text{NH}_2\text{OH}$  in place of  $\text{NH}_2\text{OH}\cdot\text{HCl}$  (Supporting Information), nitriles of **14** were converted to bis-amidine **17**. The Boc group was removed using ethanolic HCl to obtain **18**. Compounds **19**–**24** were synthesized utilizing the similar synthetic procedures as described for **18** by using nicotinic acid or isonicotinic acid intermediate (**13**) and coupling with different alkyl amines. The results of selected compounds are summarized in Table 1.

Most of these  $\text{R}^1$  modifications (Table 1) lead to reduced potency, while some of the  $\text{R}^2$  modifications as in **23** and **24** exhibited similar inhibition as **10**. Among these two compounds, **24** exhibited a better selectivity profile. To understand this structure–activity relationship (SAR) paradox, we determined the crystallographic binding mode of **24** (PDB code: 4JZL; Figure 2f). Its crystal structure revealed an unexpected inverse binding mode in comparison to the pyridyl sulfonamides. In the case of pyridyl sulfonamides (**10**), the 3-pyridyl sulfonamide substituents ( $\text{R}^1$  in Table 1) occupy a region close to the Cys42–Cys58

### Scheme 1. Synthetic Scheme of 4,4'-(Pyridine-2,6-diylbis(oxy))dibenzimidamide Derivatives<sup>a</sup>



<sup>a</sup>Reagents and conditions: (a)  $\text{K}_2\text{CO}_3$ , DMF, 75 °C. (b)  $\text{NH}_2\text{OH}\cdot\text{HCl}$ , DIPEA, EtOH, 6 h, 85 °C. (c)  $\text{Ac}_2\text{O}$ , AcOH, RT. (d)  $\text{H}_2$  at balloon pressure, 10% Pd/C, AcOH, 30 °C. (e) Zn powder, AcOH, 35 °C. (f) 4-Fluorobenzene sulfonylchloride, DIPEA, THF, RT.

Scheme 2. Synthetic Scheme of 2,6-Bis(4-carbamimidoylphenoxy)nicotinamide Derivatives<sup>a</sup>

<sup>a</sup>Reagents and conditions: (a)  $K_2CO_3$ , DMF, 75 °C. (b) LiOH, THF, MeOH, 2 h, 15–20 °C. (c) *tert*-Butyl ((1*R*,4*R*)-4-aminocyclohexyl)carbamate, PyBop, DIPEA, DMF, RT. (d) Aq.  $NH_2OH$ , EtOH, 4 h, 75 °C. (e)  $Ac_2O$  in AcOH, RT. (f) Zn powder, AcOH, RT. (g)  $HCl(g)$ –EtOH at 5–10 °C.

Table 2. Analysis of Selected Compounds for Cellular Activity on PC-3 and DU-145, Aqueous Solubility, and Metabolic Stability

ID	% cytotoxicity at 10 $\mu M$		% inhibition at 10 $\mu M^a$				aq sol <sup>a</sup> ( $\mu M$ )	MLM stability <sup>a</sup> (% parent remaining)		
	PC-3	DU-145	PC-3		DU-145			pH 7.4	20 min	40 min
			migration	invasion	migration	invasion				
8	0	0	65 $\pm$ 2.4	60 $\pm$ 0.8	69 $\pm$ 0.8	61 $\pm$ 2.4	194 $\pm$ 4	89.0 $\pm$ 2.3	86.5 $\pm$ 10.5	
10	20	20	39 $\pm$ 2.1	42 $\pm$ 0.9	59 $\pm$ 0.8	47 $\pm$ 1.1	191 $\pm$ 4	76.4 $\pm$ 2.5	73.2 $\pm$ 5.5	
24	1	0	53 $\pm$ 1.8	42 $\pm$ 5.9	65 $\pm$ 1.1	69 $\pm$ 2.0	196 $\pm$ 2	100 $\pm$ 10.3	95.6 $\pm$ 11.2	

<sup>a</sup>Values represent mean  $\pm$  SD.

disulfide-bridge, but in this case (**24**), the  $R^1$  moiety *trans*-4-aminocyclohexane orients away from that region, and instead, the P3/P4 benzamidine moiety of **24** occupies the region close to Cys42–Cys58 disulfide-bridge making two polar backbone contacts with His57 and Cys58 (Figure 2f). Molecular modeling suggests that compounds including **18–21** with  $R^1$  substituents are likely to sterically interfere with either Phe99 or Trp215–Gly216 potentially leading to reduced matriptase inhibition.

After establishing the SAR for matriptase inhibition and selectivity against other proteases, selected compounds were studied for their effect on matriptase expressing prostate carcinoma cell lines (PC-3 and DU-145), solubility, and metabolic stability in mouse liver microsomes (MLM) (Table 2).

Compounds **8** and **24** were not cytotoxic and all tested compounds displayed good inhibition of invasion and migration in PC-3 and DU-145 cells. All three compounds also showed high aqueous solubility and good metabolic stability.

In conclusion, we have optimized a pyridyl bis(oxy)-benzamidine series and achieved high potency toward matriptase ( $K_i = 0.04 \mu M$ ) and desirable selectivity over other proteases, cellular activity, solubility, and metabolic stability. The optimized compounds with sulfonamide and isonicotinamide derivatives have the potential to be used as anti-invasive agents.

## ■ ASSOCIATED CONTENT

### § Supporting Information

Experimental details for synthesis, protein expression, assay methods, modeling, and crystallography. This material is available free of charge via the Internet at <http://pubs.acs.org>.

## ■ AUTHOR INFORMATION

### Corresponding Author

\*(M.R.) Tel: +91 80 7102 5444. Fax: +91 80 2852 6285. E-mail: [murali\\_r@aurigene.com](mailto:murali_r@aurigene.com).

### Funding

We gratefully acknowledge Orion Corporation for funding this research.

### Notes

The authors declare the following competing financial interest(s): All authors are current or former employees of Aurigene Discovery Technologies Limited or Orion Corporation as indicated.

## ■ REFERENCES

- (1) Coghlin, C.; Murray, G. I. Current and emerging concepts in tumour metastasis. *J. Pathol.* **2010**, *222*, 1–15.
- (2) Duffy, M. J. Do proteases play a role in cancer invasion and metastasis? *Eur. J. Cancer Clin. Oncol.* **1987**, *23*, 583–589.
- (3) Liotta, L. A.; Stetler-Stevenson, W. G. Tumor invasion and metastasis: an imbalance of positive and negative regulation. *Cancer Res.* **1991**, *51*, 5054s–5059s.

- (4) Deryugina, E. I.; Quigley, J. P. Matrix metalloproteinases and tumor metastasis. *Cancer Metastasis Rev.* **2006**, *25*, 9–34.
- (5) Bonfil, R. D.; Cher, M. L. The role of proteolytic enzymes in metastatic bone disease. *IBMS BoneKEy* **2011**, *8*, 16–36.
- (6) Naglich, J. G.; Jure-Kunkel, M.; Gupta, E.; Fagnoli, J.; Henderson, A. J.; Lewin, A. C.; Talbott, R.; Baxter, A.; Bird, J.; Savopoulos, R.; Wills, R.; Kramer, R. A.; Trail, P. A. Inhibition of angiogenesis and metastasis in two murine models by the matrix metalloproteinase inhibitor, BMS-27529. *Cancer Res.* **2001**, *61*, 8480–8485.
- (7) Ertongur, S.; Lang, S.; Mack, B.; Wosikowski, K.; Muehlenweg, B.; Gires, O. Inhibition of the invasion capacity of carcinoma cells by WX-UK1, a novel synthetic inhibitor of the urokinase-type plasminogen activator system. *Int. J. Cancer* **2004**, *110*, 815–824.
- (8) Steinmetzer, T.; Schweinitz, A.; Stürzebecher, A.; Dönnecke, D.; Uhland, K.; Schuster, O.; Steinmetzer, P.; Müller, F.; Friedrich, R.; Than, M. E.; Bode, W.; Stürzebecher, J. Secondary amides of sulfonylated 3-amidinophenylalanine. New potent and selective inhibitors of matriptase. *J. Med. Chem.* **2006**, *49*, 4116–4126.
- (9) List, K.; Haudenschield, C. C.; Szabo, R.; Chen, W.; Wahl, S. M.; Swaim, W.; Engelholm, L. H.; Behrendt, N.; Bugge, T. H. Matriptase/MT-SP1 is required for postnatal survival, epidermal barrier function, hair follicle development, and thymic homeostasis. *Oncogene* **2002**, *21*, 3765–3779.
- (10) Hooper, J. D.; Clements, J. A.; Quigley, J. P.; Antalis, T. M. Type II transmembrane serine proteases. *J. Biol. Chem.* **2001**, *276*, 857–860.
- (11) Tsui, K. H.; Chang, P. L.; Feng, T. H.; Chung, L. C.; Hsu, S. Y.; Juang, H. H. Down-regulation of matriptase by overexpression of bikunin attenuates cell invasion in prostate carcinoma cells. *Anticancer Res.* **2008**, *28*, 1977–1983.
- (12) List, K.; Bugge, T. H.; Szabo, R. Matriptase: potent proteolysis on the cell surface. *Mol. Med.* **2006**, *12*, 1–7.
- (13) Milner, J. M.; Patel, A.; Davidson, R. K.; Swingler, T. E.; Désilets, A.; Young, D. A.; Kelso, E. B.; Donell, S. T.; Cawston, T. E.; Clark, I. M.; Ferrell, W. R.; Plevin, R.; Lockhart, J. C.; Leduc, R.; Rowan, A. D. Matriptase is a novel initiator of cartilage matrix degradation in osteoarthritis. *Arthritis Rheum.* **2010**, *61*, 1955–1966.
- (14) Netzel-Arnett, S.; Buzza, M. S.; Shea-Donohue, T.; Désilets, A.; Leduc, R.; Fasano, A.; Bugge, T. H.; Antalis, T. M. Matriptase protects against experimental colitis and promotes intestinal barrier recovery. *Inflamm. Bowel Dis.* **2012**, *18*, 1303–1314.
- (15) Beaulieu, A.; Gravel, É.; Cloutier, A.; Marois, I.; Colombo, É.; Désilets, A.; Verreault, C.; Leduc, R.; Marsault, É.; Richter, M. V. Matriptase proteolytically activates influenza virus and promotes multicycle replication in the human airway epithelium. *J. Virol.* **2013**, *87*, 4237–4251.
- (16) Baron, J.; Tarnow, C.; Mayoli-Nüssle, D.; Schilling, E.; Meyer, D.; Hammami, M.; Schwalm, F.; Steinmetzer, T.; Guan, Y.; Garten, W.; Klenk, H. D.; Böttcher-Friebertshäuser, E. Matriptase, HAT, and TMPRSS2 activate the hemagglutinin of H9N2 influenza A viruses. *J. Virol.* **2013**, *87*, 1811–1820.
- (17) Mika, S.; Hiroshi, K.; Naohiro, K.; Yasushi, S.; Mitsuki, S.; Chen-Yong, L.; Robert, B. D.; Toshihiko, T. Inhibition of tumor invasion by genomic down-regulation of matriptase through suppression of activation of receptor-bound Pro-urokinase. *J. Biol. Chem.* **2004**, *279*, 14899–14908.
- (18) Sheau-Ling, L.; Robert, B. D.; Chen-Yong, L. Activation of hepatocyte growth factor and urokinase/plasminogen activator by matriptase, an epithelial membrane serine protease. *J. Biol. Chem.* **2000**, *275*, 36720–36725.
- (19) Enyedy, I. J.; Lee, S. L.; Kuo, A. H.; Dickson, R. B.; Lin, C. Y.; Wang, S. Structure-based approach for the discovery of bis-benzamidines as novel inhibitors of matriptase. *J. Med. Chem.* **2001**, *44*, 1349–1355.
- (20) Schweinitz, A.; Dönnecke, D.; Ludwig, A.; Steinmetzer, P.; Schulze, A.; Kotthaus, J.; Wein, S.; Clement, B.; Steinmetzer, T. Incorporation of neutral C-terminal residues in 3-amidinophenylalanine-derived matriptase inhibitors. *Bioorg. Med. Chem. Lett.* **2009**, *19*, 1960–1965.
- (21) Colombo, É.; Désilets, A.; Duchêne, D.; Chagnon, F.; Najmanovich, R.; Leduc, R.; Marsault, E. Design and synthesis of potent, selective inhibitors of matriptase. *ACS Med. Chem. Lett.* **2012**, *3*, 530–534.
- (22) Friedrich, R.; Fuentes-Prior, P.; Ong, E.; Coombs, G.; Hunter, M.; Oehler, R.; Pierson, D.; Gonzalez, R.; Huber, R.; Bode, W.; Madison, E. L. Catalytic domain structures of MT-SP1/matriptase, a matrix-degrading transmembrane serine proteinase. *J. Biol. Chem.* **2002**, *277*, 2160–2168.
- (23) Phillips, G.; Davey, D. D.; Eagen, K. A.; Koovakkat, S. K.; Liang, A.; Ng, H. P.; Pinkerton, M.; Trinh, L.; Whitlow, M.; Beatty, A. M.; Morrissey, M. M. Design, synthesis, and activity of 2,6-diphenoxypyridine-derived factor Xa inhibitors. *J. Med. Chem.* **1999**, *42*, 1749–1756.
- (24) Friedrich, R.; Steinmetzer, T.; Huber, R.; Stürzebecher, J.; Bode, W. The methyl group of N(α)(Me)Arg-containing peptides disturbs the active-site geometry of thrombin, impairing efficient cleavage. *J. Mol. Biol.* **2002**, *316*, 869–874.
- (25) Maignan, S.; Guilloteau, J. P.; Pouzieux, S.; Choi-Sledeski, Y. M.; Becker, M. R.; Klein, S. I.; Ewing, W. R.; Pauls, H. W.; Spada, A. P.; Mikol, V. Crystal structures of human factor Xa complexed with potent inhibitors. *J. Med. Chem.* **2000**, *43*, 3226–3232.
- (26) *WaterMap*, version 1.2; Schrödinger, LLC: New York, 2012.
- (27) Brodney, M. A.; Barreiro, G.; Ogilvie, K.; Hajos-Korcsok, E.; Murray, J.; Vajdos, F.; Ambroise, C.; Christoffersen, C.; Fisher, K.; Lanyon, L.; Liu, J.; Nolan, C. E.; Withka, J. M.; Borzilleri, K. A.; Efremov, I.; Oborski, C. E.; Varghese, A.; O'Neill, B. T. Spirocyclic sulfamides as -secretase 1 (BACE-1) inhibitors for the treatment of Alzheimer's disease: utilization of structure based drug design, WaterMap, and CNS penetration studies to identify centrally efficacious inhibitors. *J. Med. Chem.* **2012**, *55*, 9224–9239.